Catalysis Today 183 (2012) 72–78

Contents lists available at SciVerse ScienceDirect

Catalysis Today

journal homepage: www.elsevier.com/locate/cattod

Structure sensitivity in the hydrogenation of unsaturated hydrocarbons over Rh nanoparticles

Xian-Yang Quek, Yejun Guan, Emiel J.M. Hensen*

Laboratory of Inorganic Materials Chemistry, Schuit Institute of Catalysis, Eindhoven University of Technology, P.O. Box 513, 5600 MB Eindhoven, The Netherlands

ARTICLE INFO

Article history:
Received 3 July 2011
Received in revised form 12 October 2011
Accepted 13 October 2011
Available online 21 November 2011

Keywords:
Rhodium
Nanoparticles
Hydrogenation
Particle size

ABSTRACT

A series of Rh nanoparticles with sizes between 3.5 and 11.4 nm were synthesized in the presence of polyvinylpyrrolidone and evaluated for their performance as catalysts in the hydrogenation of phenylacetylene and 1-octene. The reaction is zeroth order in the reactant for phenylacetylene and 1-octene. The catalytic activity increased with Rh particle size in the hydrogenation of phenylacetylene, whereas the activity in 1-octene hydrogenation did not depend on particle size. The possible explanations for this different particle size behavior are discussed.

1. Introduction

The recent advancement in colloidal chemistry has allowed more effective control of the size and morphology of metallic nanoparticles with many applications in the field of catalysis [1–7]. Among the various methods employed to prepare colloidal nanoparticles, polyol reduction of metal salts in the presence of polyvinylpyrrolidone (PVP) is one of the most common methods to synthesize mono-dispersed nanoparticles with a narrow size distribution [1–3]. This approach has been shown to be effective in controlling both the size [8,9] and shape [10] of the particles. For instance, PVP stabilized Rh nanoparticles with sizes between 2 and 11 nm and were prepared by the group of Somorjai [8,9]. In addition, Rh nanoparticles of different shapes were successfully synthesized including cube, tetrahedral, polyhedral, multipods, ultrathin plates, starfish-like and concave cubes Rh nanocrystals [10]. One advantage of using colloidal nanoparticles in fundamental catalysis studies is to decouple the effect of the metal-support interaction from the intrinsic effect of the particle size on the activity of the surface metal atoms. Thus, the use of colloidal nanoparticles offers opportunities to study the intrinsic structure–activity relationship of metal nanoparticles [1–6].

Based on the extensive work on Pt catalysts in the 1960s and early 1970s Boudart classified reactions as structure sensitive or structure insensitive [11]. For instance, the rate of alkane hydrogenolysis will strongly depend on the Pt particle size in contrast to the rate of olefin hydrogenation, which is structure insensitive [2,4]. Che and Bennette classified structure sensitive/insensitive-particle size relationship into three different types, where rate normalized per exposed metal surface atom, decreases, remained constant or increases with increasing particle size [12].

In the last decade or so a firm theoretical basis about surface reactivity of metals has been developed to understand structure sensitivity [13–15]. Van Santen reviewed the issue of structure sensitivity in detail from the viewpoint of reactivity of molecules at metal surface ensembles with different surface metal atom coordination and topology [14]. Broadly speaking, structure sensitivity depends on the type of bond to be activated during the rate limiting elementary reaction step at the surface. When this step involves the formation or cleavage of a π-bond as is the case in the activation of CO, NO or N_2, the rate will increase with increasing particle size. The reason lies in the much lower activation energy for such reactions over step-edge sites than over terraces, which is mainly related to the absence of surface metal atom sharing of the dissociating atoms. Activation of σ-bonds such as the dissociative adsorption of methane (C–H bond activation) occurs over a single surface metal atom with a late transition state. In this case, Brønsted–Evans–Polanyi (BEP) considerations predict that lower surface metal atom coordination results in higher reactivity due to stabilization of the transition and final states because of increased adsorption energies of the dissociating molecule. Accordingly, one predicts that smaller particles are more active in σ-bond cleavage. In contrast, the reverse reaction that forms a σ-bond such as the case for hydrogenation is characterized by an early transition state. This implies that a stabilization of the initial state by a more reactive

* Corresponding author. Tel.: +31 40 2475178; fax: +31 40 2455054.
E-mail address: e.j.m.hensen@tue.nl (E.J.M. Hensen).

0920-5861/$ – see front matter © 2011 Elsevier B.V. All rights reserved.
doi:10.1016/j.cattod.2011.10.014

surface metal atom will also stabilize the transition state further. BEP considerations dictate then that the formation of a σ-bond does not strongly depend on the particle size. As such, this explains the structure insensitivity of metals such as Pt in olefin hydrogenation.

The influence of metal particle size on the hydrogenation of olefinic bonds is of great interest due to the importance of hydrogenation processes in the petrochemical, fine chemical and food industries [16,17]. Although hydrogenation is argued to be structure insensitive [14], contradicting reports can be found in literature. Some reports claim indeed that the hydrogenation is independent of particle size [2,18–21], whereas others show that the activity increases with particle size [22–31].

Structure insensitivity in hydrogenation has mainly been reported for Pt and Pd catalysts. When Pt particles increase from 1 to 7 nm, the catalytic activity was found to be unaffected in the hydrogenation of ethylene [2,18,19] and cyclohexene [2,20]. For Pd particles between 6 and 11 nm, Semagina et al. [21] found that the activity for 1-hexyne hydrogenation did not depend on the particle size. In contrast, the activity increased with Pt nanoparticle size (1–7 nm) in the hydrogenation of cinnamaldehyde [22,23], crotonaldehyde [24] and cyclohexanone [25]. Higher activity was also observed for the hydrogenation of 1,3-butadiene [26], 2-methyl-3-butyl-2-ol [27] and allyl alcohol [28] with increasing Pd particle size from 1 to 13 nm. Although the effect of particle size in hydrogenation for Ru and Rh is less well documented, increasing catalytic activities with particle size have also been observed. Campbell et al. [29] reported increasing activities for 1,3-cyclohexadiene hydrogenation with increasing Ru nanoparticle size (1–3 nm). In the hydrogenation of ethyl pyruvate [30] and xylene [31], increasing the Rh particle size from 1–2 nm to 2–8 nm resulted in higher activity.

Despite Rh being an excellent hydrogenation catalyst, a comprehensive study on the particle size effect for Rh is still lacking. The aim of this work is to investigate whether hydrogenation of olefinic bonds is particle size dependent. PVP stabilized Rh nanoparticles from 3.5 to 11.4 nm will be synthesized and used in the hydrogenation of phenylacetylene and 1-octene.

2. Experimental

2.1. Rh nanoparticle synthesis

Polyvinylpyrrolidone (PVP, M_n = 10,000, Sigma–Aldrich) stabilized Rh nanoparticles were synthesized according to a published procedure [9]. Rh nanoparticles were prepared by reducing either rhodium(III) chloride hydrate ($RhCl_3 \cdot nH_2O$, Aldrich) or rhodium(III) acetylacetonate ($Rh(acac)_3$, Aldrich) at different temperature in ethylene glycol (EG, Merck) or 1,4-butanediol (Sigma–Aldrich). In a typical synthesis, 20 mg of $Rh(acac)_3$ and 0.11 g of PVP were dissolved in 2 mL of tetrahydrofuran (THF, Sigma–Aldrich) and 3 mL of 1,4-butanediol. The mixture was then added to 17 mL of 1,4-butanediol preheated to 220 °C and refluxed under N_2 flow for 6 h. The resultant black mixture was washed thoroughly with acetone and diethyl ether and collected by centrifugation. The isolated Rh nanoparticles were then redispersed in 3 mL deionized water. Although 1,4-butanediol and excess PVP were removed by washing, a portion of PVP will remain coordinated to the surface of the Rh nanoparticles. The only effective method of removing surface coordinated PVP without using high temperature calcination would be to use UV-ozone cleaning [32].

2.2. Characterization

Transmission electron microscopy (TEM) was performed on FEI Tecnai 20 electron microscope at an acceleration voltage of 200 kV with a LaB_6 filament. A small amount of the sample was diluted with ethanol, dispersed and dried over a carbon-coated Cu grid. Particle size distribution was calculated by measuring more than 150 particles. X-ray diffraction was measured under ambient conditions with a Bruker Endeavour D4 diffractometer using filtered Cu Kα radiation (40 kV and 40 mA). Diffraction data were recorded from 2θ from 25° to 60° at a resolution of 0.05°. X-ray photoelectron spectrometer (XPS) samples were prepared by drying the dispersed Rh nanoparticles on a silica wafer before introducing into a Thermo Scientific K-Alpha XPS equipped with a monochromatic Al Kα X-ray. For survey and region scans, constant pass energies of 160 eV and 40 eV, respectively, were used. The background pressure was 2×10^{-9} mbar. Fitting was carried out with the CasaXPS program.

2.3. Catalytic activity

Liquid phase catalytic hydrogenation experiments were carried out in a batch reactor operated at atmospheric pressure. 1 mmol of reactant being either phenylacetylene (Fluka) or 1-octene (Sigma–Aldrich), 1.6 μmol of Rh nanoparticles, 0.4 mL of deionized water and 15 mL of n-heptane were introduced into a round-bottom flask. Pure molecular hydrogen was bubbled through the flask at a flow rate of 30 mL/min for 5 min under vigorous magnetic stirring (800 rpm). The reaction was initiated by immersing the flask into an oil bath maintained at 70 °C. The reaction time was 4 h for phenylacetylene and 1 h for 1-octene. Aliquots of 100 μL liquid were extracted from the reactor at regular intervals (1 h for phenylacetylene and 15 min for 1-octene) and diluted with ethanol before analysis. The liquid sample was analyzed by gas chromatography (QP5050, Shimadzu) equipped with a Rxi-5ms capillary column (30 m × 0.25 mm × 0.5 μm) and a flame ionization detector (FID).

The turn over frequency (TOF) is calculated based on the following equations:

$$\mathrm{TOF} = \frac{\text{moles reacted}}{\text{mol Rh}_{\text{surface}} \times \text{reaction time}}$$

with the number of mol $Rh_{surface}$ = mol Rh × D and D being the dispersion.

The dispersion (D) was calculated assuming spherical shapes by using the formula described by Scholten et al. [33]:

$$D = 10^{21} \times \frac{6 \times M \times \rho_{\text{site}}}{d_p \times N_{\text{AV}} \times \rho_{\text{metal}}}$$

with M being the atomic weight of Rh, ρ_{site} the surface density, ρ_{metal} the density of metal, N_{Av} the Avogadro's number.

3. Results and discussion

3.1. Catalyst characterizations

Our initial approach to control the size of Rh nanoparticles was to vary the PVP/Rh molar ratio and the reduction time (t_R). The PVP/Rh ratio varied from 6 to 24 and t_R varied from 5 to 120 min as summarized in Table 1. Fig. 1 shows the transmission electron micrographs and XRD patterns for Rh nanoparticles prepared using $RhCl_3$ with PVP/Rh molar ratio of 18 and 24 and t_R = 5 min. The average particle size of these PVP stabilized Rh nanoparticles from TEM analysis is 3.3 ± 0.5 nm for PVP/Rh ratios of 18 and 24, respectively. The Rh particle size estimated by applying Scherrer's equation to the Rh(1 1 1) reflection gave similar results (3.3 nm for PVP/Rh = 18 and 24). Table 1 summarizes the particle size of Rh determined by XRD and TEM when the PVP/Rh ratio and t_R were varied. Although previous studies found that the size of Pt and Pd nanoparticles can be varied by changing the PVP/Rh ratio and reduction time [34,35],

Table 1
Rh nanoparticles synthesis conditions and particle size.[a]

Rh source	Temperature (°C)	Solvent	PVP/Rh molar ratio	t_R (h)	d_{XRD} [b] (nm)	d_{TEM} [c] (nm)
$RhCl_3$	140	EG	6	5 min	2.9	2.9 ± 0.6
$RhCl_3$	140	EG	12	5 min	3.5	n.d.
$RhCl_3$	140	EG	18	5 min	3.3	3.3 ± 0.5
$RhCl_3$	140	EG	24	5 min	3.3	3.3 ± 0.5
$RhCl_3$	140	EG	6	0.5	3.4	3.0 ± 0.7
$RhCl_3$	140	EG	6	1	3.4	n.d.
$RhCl_3$	140	EG	6	2	3.4	n.d.

[a] Molecular weight of PVP used, M_n = 58,000.
[b] Particle size determine from XRD using Scherrer's equation for Rh(1 1 1) peak.
[c] Average particle size and standard deviation determined from TEM.

only small changes were found in the Rh particle size when varying these parameters. Hence, we conclude that changing Rh/PVP ratio and t_R is not a good method to obtain Rh nanoparticles with different sizes.

Previous reports suggest that changing the reduction temperature and the Rh source is able to effectively control the size of Rh nanoparticles [8,36]. Table 2 gives the results for such experiments by which Rh nanoparticles between 3.5 and 11.4 nm were obtained. Transmission electron micrographs and the corresponding particle size distributions are given in Figs. 2 and 3. Fig. 4 shows that higher reduction temperature resulted in larger Rh nanoparticles. By using $Rh(acac)_3$ instead of $RhCl_3$ under otherwise similar conditions we obtained larger particles, suggesting that the ligand is also important. Chaudret and co-workers have extensively investigated the possibilities to control the size and morphology of metallic nanoparticles by using organometallic precursor compounds [37,38]. Fig. 4 also shows that reducing $RhCl_3$ at higher temperature cannot further increase the particle size. The particle size leveled off when the reduction temperature increases from 160 °C to 190 °C. However, for $Rh(acac)_3$ the size of Rh nanoparticles can be further increased by an increase of the reduction temperature. The temperature is however limited by the boiling point of 1,4-butandiol.

TEM micrographs in Figs. 2 and 3 show that smaller Rh particles are mostly composed of spherical particles. When the particle size increase, the portion of well facetted particles increases. These well-facetted PVP stabilized Rh nanoparticles contains various polygonal shapes such as hexagons, pentagons, triangles and rhombohedra. However, no dominant shape was observed among these particles.

Fig. 5 shows the X-ray photoelectron (XP) spectra for Rh-3.5 and Rh-11.4. The spectra of these nanoparticles contain peaks at 306.5 eV and 308.0 eV, indicating the presence of Rh^0 and Rh^{3+}, respectively. We employ the distinction in these two oxidation states, although the particles may also contain Rh^+ which cannot be distinguished accurately in the XP spectra. The metallic Rh content for different particle size was determined from such XP spectra and are collected in Table 2. Although it is known that small particles are more prone to oxidation [39,40], our results indicate that there is little influence of the particle size on the oxidation state. The average content of metallic Rh was 81 ± 4%. One tentative explanation for the small decrease in metallic Rh content for smaller particles is the slight underestimation of the metallic Rh in large particles due to the surface sensitivity of XPS.

3.2. Effect of PVP/Rh ratio and reduction time

Although recently Yang et al. [41] have shown that PVP stabilized Rh nanoparticles in ionic liquid is able to effectively convert styrene into ethylbenzene, our experiments show that

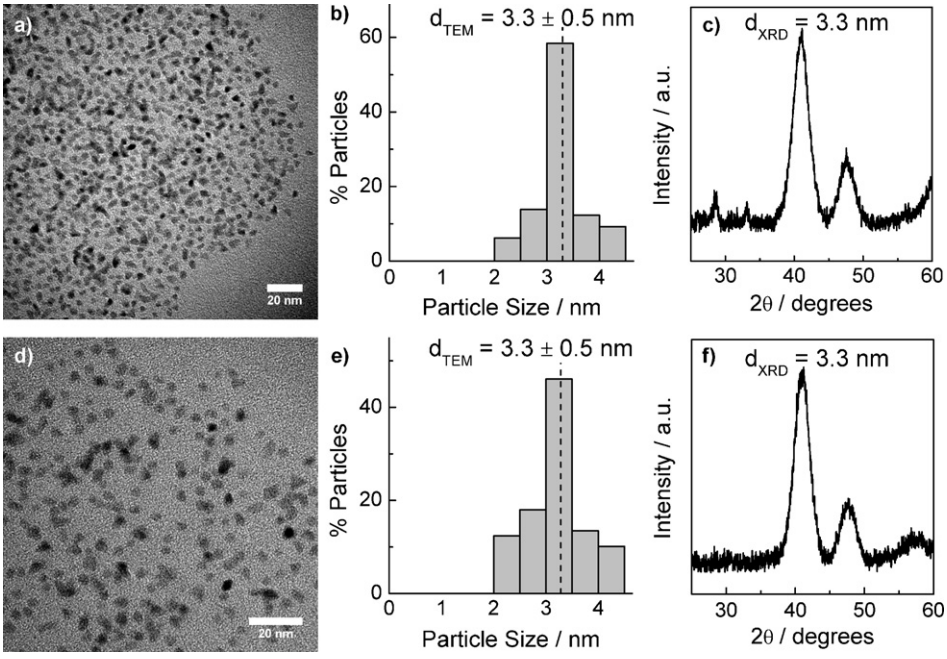

Fig. 1. PVP-stabilized Rh nanoparticles: (a, d) electron micrograph; (b, e) particle size distribution; (c, f) XRD pattern for PVP/Rh = 18 and t_R = 5 (a–c) and PVP/Rh = 24 and t_R = 5 (d–f).

Table 2
Rh nanoparticles synthesis conditions and particle size.[a]

Catalyst	Rh source	T (°C)	t_R (h)	d_p [b] (nm)	Rh conc.[c] (μg/mL)	Rh^0 content[d] (%)
Rh-3.5	$RhCl_3$	120	5 min	3.5 ± 0.6	762	79
Rh-6.4	$RhCl_3$	160	6	6.4 ± 1.3	974	79
Rh-7.0	$RhCl_3$	190	6	7.0 ± 1.1	875	76
Rh-8.1	$Rh(acac)_3$	160	6	8.1 ± 1.1	762	84
Rh-10.2	$Rh(acac)_3$	190	6	10.2 ± 2.1	905	86
Rh-11.4	$Rh(acac)_3$	220	6	11.4 ± 1.9	835	83

[a] 1,4-Butanediol as reducing agent and solvent, PVP/Rh molar ratio = 20, M_n(PVP) = 10,000.
[b] Average particle size and standard deviation determined from TEM.
[c] Determined from ICP.
[d] Determined from XPS.

phenylacetylene is predominately semi-hydrogenated to styrene with ethylbenzene as a byproduct. In our case, ethylbenzene was not the dominant product because of the use of atmospheric pressure in contrast to the work of Yang et al., who employed 50 bar H_2. Fig. 6 shows the effect of the PVP/Rh ratio on the phenylacetylene hydrogenation activity and selectivity at 75 °C. Phenylacetylene conversion remained nearly unchanged with increasing surfactant to Rh ratio (51 ± 5%). Styrene selectivity also remained constant at approximately 70 ± 1%. Similarly, increasing reduction time had only very small effect on the hydrogenation activity and selectivity, that is the phenylacetylene conversion and styrene selectivity were 48 ± 3% and 66 ± 3%, respectively, when the sample was longer reduced. These results show that particles of the same size yield comparable catalytic activities independent of the amount of PVP and the reduction time.

3.3. Time dependent hydrogenation activity and selectivity

Fig. 7 shows the activity for phenylacetylene (Fig. 7a) and 1-octene (Fig. 7b) hydrogenation with reaction time for Rh-3.5 and Rh-11.4. In the hydrogenation of phenylacetylene, conversion increases linearly with reaction time for both Rh-3.5 and Rh-11.4. This indicates a zero order reaction with respect to phenylacetylene, which was also observed by Jackson and Shaw using a Pd/C catalyst [42]. Styrene selectivity remained unchanged with time at 74 ± 3% for both catalysts. Similarly, in the hydrogenation of 1-

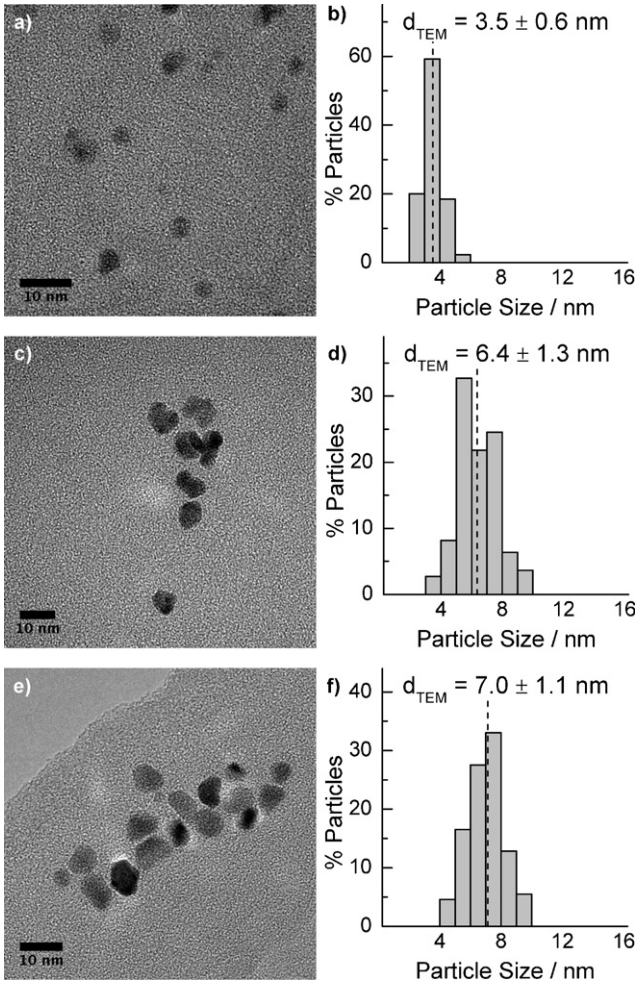

Fig. 2. Rh nanoparticles prepared using $RhCl_3$ reduced at 120 °C (a, b), 160 °C (c, d) and 190 °C (e, f): electron micrograph (a, c, e); particle size distribution (b, d, f).

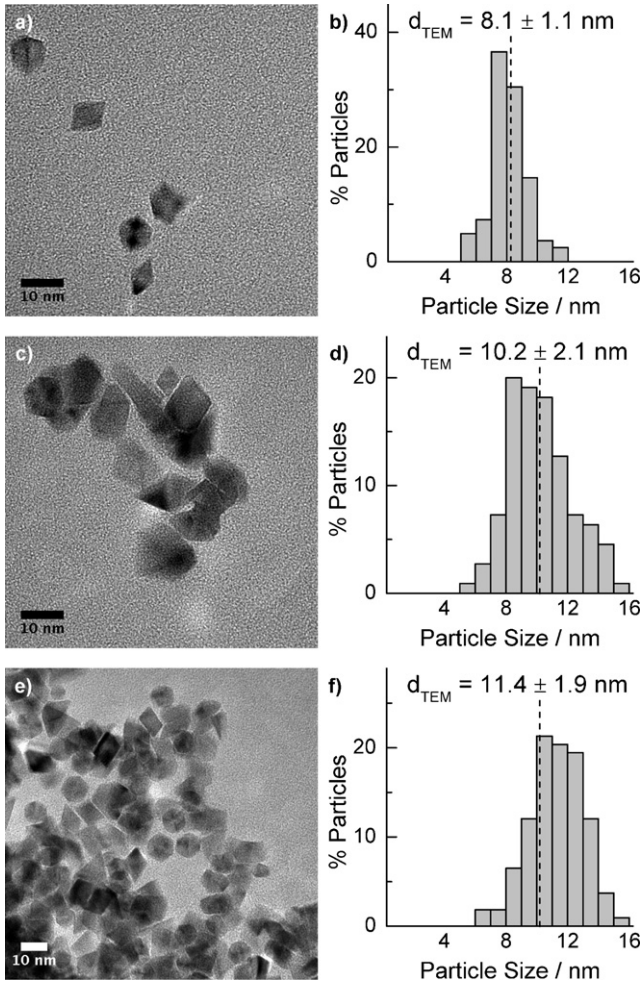

Fig. 3. Rh nanoparticles prepared using $Rh(acac)_3$ reduced at 160 °C (a, b), 190 °C (c, d) and 220 °C (e, f): electron micrograph (a, c, e); particle size distribution (b, d, f).

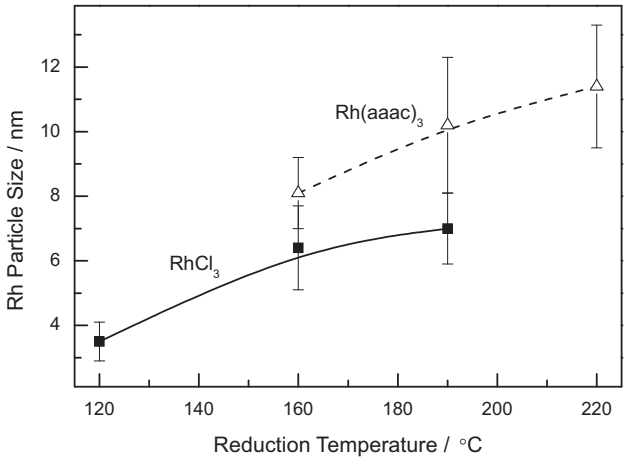

Fig. 4. Rh particle size as a function of reduction temperature.

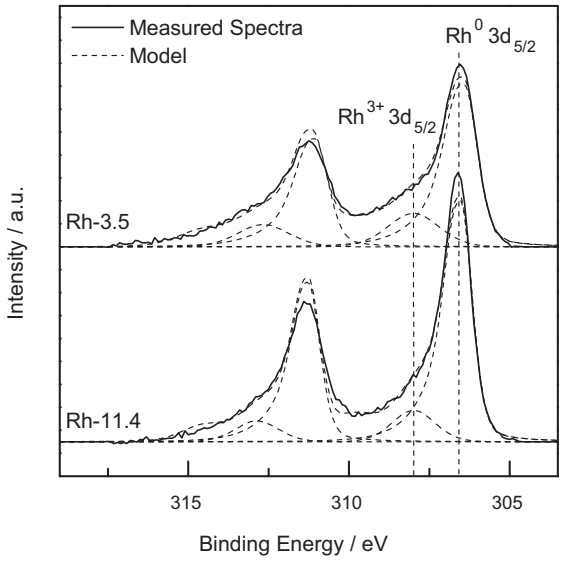

Fig. 5. X-ray photoelectron spectra of Rh nanoparticles in the Rh 3d region.

octene (Fig. 7b), it was seen that conversion increased linearly with reaction time for Rh-11.4, while a plateau was reached for Rh-3.5 at approximately 90% conversion. Hence, 1-octene hydrogenation

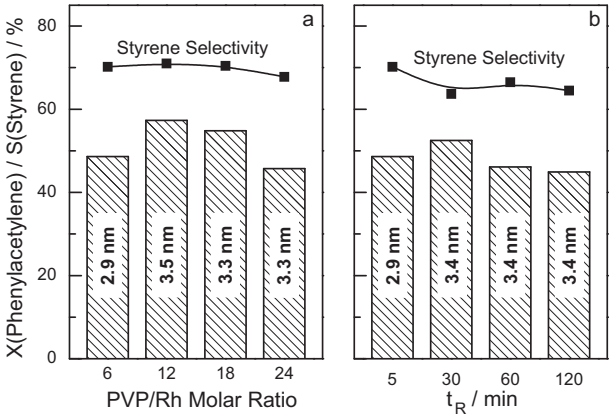

Fig. 6. Rh nanoparticle size and catalytic activity in phenylacetylene hydrogenation at 75 °C as a function of: (a) PVP/Rh ratio and (b) reduction time.

also exhibits a zero order behavior in the reactant when conversion is kept below 80%.

3.4. Effect of particle size on hydrogenation

Fig. 8 shows the effect of the Rh particle size on the turnover frequency (TOF) for the hydrogenation phenylacetylene and 1-octene calculated on the basis of the total surface Rh atoms. In the hydrogenation of phenylacetylene, it is observed that TOF increases linearly from 250 to 650 h^{-1} when the Rh particle size increases from 3.5 to 11.4 nm. However, for 1-octene the TOF remained at about 10000 h^{-1} independent of the Rh particle size.

An explanation for the different dependency of the activity on the particle size for the hydrogenation of phenylacetylene and 1-octene relates to the adsorption mode of the reactant on the surface of the Rh nanoparticle. It is well established that the electron-rich benzene ring prefers to adsorb in a planar mode to metal surfaces [43]. Hence, the adsorption of phenylacetylene would require a certain ensemble of metal atoms. Accordingly, larger particles with larger terrace surface planes may favor adsorption of the phenyl ring, thus increasing the catalytic activity. In contrast, the alkyl tail of 1-octene will hardly interact with the metal surface, as for instance observed for the adsorption of 1-hexene [43]. Therefore, the adsorption of 1-octene requires a smaller ensemble of metal atoms compared to phenylacetylene and one does not expect large changes in the hydrogenation activity

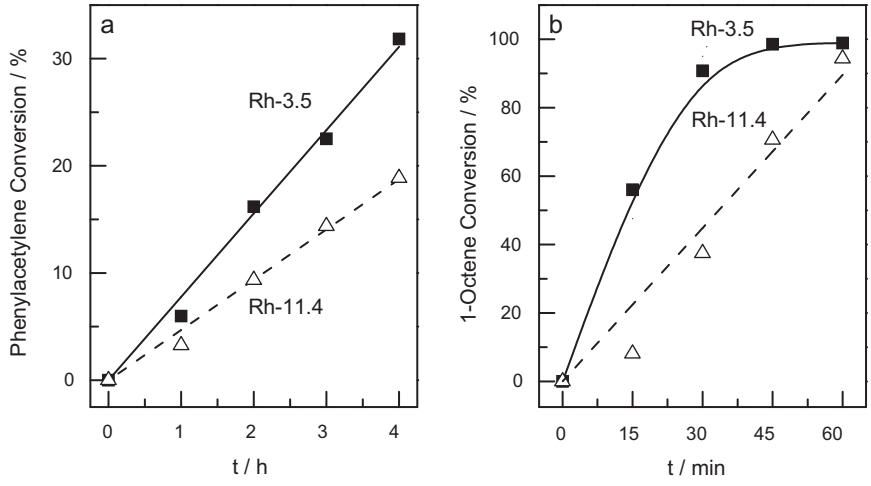

Fig. 7. Hydrogenation of: (a) phenylacetylene and (b) 1-octene over Rh-3.5 and Rh-11.4 as a function of time.

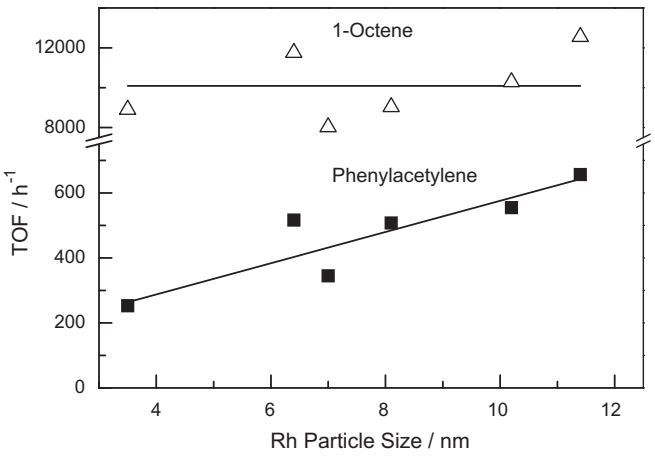

Fig. 8. Effect of Rh particle size on the TOF of phenylacetylene and 1-octene hydrogenation.

with the change in the particle size as predicted by modern insights into surface reactivity.

Another possible explanation for the different trend with increasing particle size for the hydrogenation of phenylacetylene and 1-octene could be a difference in the rate limiting steps. The general accepted mechanism for hydrogenation follows the Horiuti-Polanyi mechanism, which involves (i) adsorption of the unsaturated bond onto the catalyst surface, (ii) activation of the unsaturated bond and (iii) stepwise hydrogen addition to the substrate followed by (iv) desorption [44]. For the hydrogenation of phenylacetylene, the increasing activity with particle size may suggest that the activation of the triple bond is the rate limiting step. It has indeed been shown that the activation of unsaturated bonds proceeds more facile on larger particles [14]. In the other case where the hydrogenation of 1-octene is independent of particle size, stepwise addition of H to 1-octene will be the rate limiting step as the formation of σ-bond is known to be independent of particle size [14]. One possible explanation for the suggestion of triple bond activation in phenylacetylene to be rate limiting lies in the opposing requirements for the adsorption of the benzene ring and the activation of phenylacetylene. In the activation of the triple bond, the hybridization of the alkyne carbons will change from sp to sp^2, producing a phenylethylene as shown in Scheme 1. As a result of this, the benzene ring is no longer planar to the surface due to steric reasons [45]. Since benzene prefers to adsorb on the metal surface in a planar manner, the inclined position of the benzene ring during alkyne activation of phenylacetylene may hinder the activation of the triple bond. This will increase the activation energy barrier. A similar train of thought does not apply to the activation of 1-octene, because the alkyl chain does not have to be adsorbed on the metal surface. Another explanation for the difference in rate limiting step could be related to the substituent group attached to the unsaturated C–C bond (π-bond). Previous experimental and theoretical studies of phenylacetylene adsorption found that the interaction between the π-system of the benzene ring and triple bond produce an increase in electron density at the alkyne carbon atoms

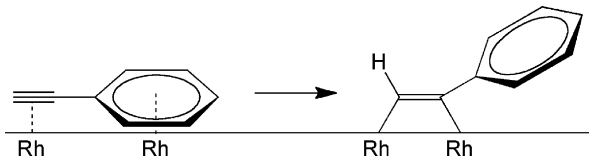

Scheme 1. Activation of adsorbed phenylacetylene on Rh surface from sp to sp^2 hybridization.

[46]. Hence, the activation of the stabilized triple bond in phenylacetylene can be argued to be more difficult than the activation of the double bond in 1-octene.

Literature data were compared in order to determine the most important factor contributing to the particle size dependence during hydrogenation. Earlier, it has been reported that hydrogenation is insensitive for ethylene [2,18,19], cyclohexene [2,20] and 1-hexyne [21]. In these cases, unsaturated C–C bond is attached to a H atom or an alkyl group. Particle size dependence was reported for hydrogenation of an unsaturated C-heteroatom bond or a C–C bond attached to a group with high electron density. Example reactants of this type are cinnamaldehyde [22,23], crotonaldehyde [24], cyclohexanone [25], 2-methyl-3-butyl-2-ol [27] and allyl alcohol [28], 1,3-cyclohexadiene [29], ethyl pyruvate [30], 1,3-butadiene [26] and xylene [31]. For hydrogenation of relatively small molecules such as 1,3-butadiene, ethyl pyruvate and crotonaldehyde, the increase in activity with particle size cannot be explained by the ensemble effect. Hence, we expect that in this case the difference in the rate limiting step has a more significant influence on the particle size dependence than the adsorption requirement. However, with such small molecules, we cannot differentiate between the particle size effect as a consequence of the change in hybridization or the substituent group attached to the unsaturated bond, because these molecules also contain an electron rich group, which prefers to be adsorbed on the surface. For cyclohexanone, the change in hybridization from sp^2 to sp^3 during the C=O activation has little influence on the adsorption of the attached cyclohexane, since it is not electron rich and does not need to be adsorbed on the metal surface in a planar manner. Therefore, the electron rich oxygen could have increased the electron density at the C=O bond and stabilized it. Hence, we postulate that the substituent group attached to the unsaturated bond is the most important factor, which determines whether the hydrogenation activity of a reactant containing unsaturated C–C bonds will depend on the metal particle size.

4. Conclusion

Size control of Rh nanoparticles stabilized by PVP is only possible to a very limited extent by varying the Rh to PVP ratio and reduction time. Rh nanoparticles of similar size exhibited similar activity in the semihydrogenation of phenylacetylene independent of the PVP/Rh ratio and reduction time. With variation of the reduction temperature and Rh source, Rh nanoparticles between 3.5 and 11.4 nm were obtained. For PVP stabilized Rh nanoparticles catalyzed hydrogenation of phenylacetylene and 1-octene, we found zero order behavior with respect to the reactants. In the hydrogenation of phenylacetylene, activity was found to increase with increasing Rh particle size, but for 1-octene the activity remained constant. The dependence of the hydrogenation activity on the Rh metal particle size was proposed to be due to the difference in the adsorption site requirement (large surface ensemble for phenyl adsorption) and in the rate limiting step. We postulate that the most significant factor influencing the structure sensitivity in hydrogenation is due to the difference in rate limiting step. For phenylacetylene hydrogenation, the activation of the unsaturated π-bond is the rate limiting step. For 1-octene, the formation of the C–H σ-bond is the rate limiting step. The substituent group attached to the unsaturated bond is suspected to have influenced the rate limiting step.

Acknowledgements

The authors thank the National Research School Combination on Catalysis for financial support and the Soft Matter Cryo-TEM

Research Unit for access to the TEM facility. We thank Adelheid Elemans for the elemental analysis.

References

[1] A.R. Tao, S. Habas, P.D. Yang, Small 4 (2008) 310–325.
[2] G.A. Somorjai, J.Y. Park, Top. Catal. 49 (2008) 126–135.
[3] B. Lim, Y.N. Xia, Angew. Chem. Int. Ed. 50 (2011) 76–85.
[4] G.A. Somorjai, C. Aliaga, Langmuir 26 (2010) 16190–16203.
[5] Y.J. Xiong, B. Wiley, Y.N. Xia, Angew. Chem. Int. 46 (2007) 7157–7159.
[6] N. Semagina, L. Kiwi-Minsker, Cat. Rev. Sci. Eng. 51 (2009) 147–217.
[7] N. Yan, C.X. Xiao, Y. Kou, Coord. Chem. Rev. 254 (2010) 1179–1218.
[8] M.E. Grass, S.H. Joo, Y.W. Zhang, G.A. Somorjai, J. Phys. Chem. C 113 (2009) 8616–8623.
[9] M.E. Grass, Y.W. Zhang, D.R. Butcher, J.Y. Park, Y.M. Li, H. Bluhm, K.M. Bratlie, T.F. Zhang, G.A. Somorjai, Angew. Chem. Int. 47 (2008) 8893–8896.
[10] Y. Xia, Y.J. Xiong, B. Lim, S.E. Skrabalak, Angew. Chem. Int. 48 (2009) 60–103.
[11] M. Boudart, Advances in Catalysis, vol. 20, Academic Press, 1969, pp. 153–166.
[12] M. Che, C.O. Bennett, Advances in Catalysis, vol. 36, Academic Press, 1989, pp. 55–172.
[13] K. Honkala, A. Hellman, I.N. Remediakis, A. Logadottir, A. Carlsson, S. Dahl, C.H. Christensen, J.K. Norskov, Science 307 (2005) 555–558.
[14] R.A. Van Santen, Acc. Chem. Res. 42 (2008) 57–66.
[15] R.A. van Santen, M. Neurock, S.G. Shetty, Chem. Rev. 110 (2010) 2005–2048.
[16] C.X. Xiao, H.Z. Wang, X.D. Mu, Y. Kou, J. Catal. 250 (2007) 25–32.
[17] C. Zhao, H.Z. Wang, N. Yan, C.X. Xiao, X.D. Mu, P.J. Dyson, Y. Kou, J. Catal. 250 (2007) 33–40.
[18] R.M. Rioux, H. Song, J.D. Hoefelmeyer, P. Yang, G.A. Somorjai, J. Phys. Chem. B 109 (2005) 2192–2202.
[19] H. Song, R.M. Rioux, J.D. Hoefelmeyer, R. Komor, K. Niesz, M. Grass, P.D. Yang, G.A. Somorjai, J. Am. Chem. Soc. 128 (2006) 3027–3037.
[20] R.M. Rioux, B.B. Hsu, M.E. Grass, H. Song, G.A. Somorjai, Catal. Lett. 126 (2008) 10–19.
[21] N. Semagina, A. Renken, L. Kiwi-Minsker, J. Phys. Chem. C 111 (2007) 13933–13937.
[22] A.J. Plomp, H. Vuori, A.O.I. Krause, K.P. de Jong, J.H. Bitter, Appl. Catal. A 351 (2008) 9–15.
[23] Z. Guo, Y.T. Chen, L.S. Li, X.M. Wang, G.L. Haller, Y.H. Yang, J. Catal. 276 (2010) 314–326.
[24] M. Grass, R. Rioux, G. Somorjai, Catal. Lett. 128 (2009) 1–8.
[25] K.A. Manbeck, N.E. Musselwhite, L.M. Carl, C.A. Kauffman, O.D. Lyons, J.K. Navin, A.L. Marsh, Appl. Catal. A 384 (2010) 58–64.
[26] J. Silvestre-Albero, G. Rupprechter, H.J. Freund, Chem. Commun. (2006) 80–82.
[27] N. Semagina, A. Renken, D. Laub, L. Kiwi-Minsker, J. Catal. 246 (2007) 308–314.
[28] O.M. Wilson, M.R. Knecht, J.C. Garcia-Martinez, R.M. Crooks, J. Am. Chem. Soc. 128 (2006) 4510–4511.
[29] P.S. Campbell, C.C. Santini, F. Bayard, Y. Chauvin, V. Colliere, A. Podgorsek, M.F.C. Gomes, J. Sa, J. Catal. 275 (2010) 99–107.
[30] F. Hoxha, N. van Vegten, A. Urakawa, F. Krurneich, T. Mallat, A. Baiker, J. Catal. 261 (2009) 224–231.
[31] H.B. Pan, C.M. Wai, J. Phys. Chem. C 114 (2010) 11364–11369.
[32] C. Aliaga, J.Y. Park, Y. Yamada, H.S. Lee, C.-K. Tsung, P. Yang, G.A. Somorjai, J. Phys. Chem. C 113 (2009) 6150–6155.
[33] J.J.F. Scholten, A.P. Pijpers, A.M.L. Hustings, Cat. Rev. Sci. Eng. 27 (1985) 151–206.
[34] T. Iwamoto, K. Matsumoto, T. Matsushita, M. Inokuchi, N. Toshima, J. Colloid Interface Sci. 336 (2009) 879–888.
[35] N. Zakarina, E. Bekturov, Chin. J. Catal. 29 (2008) 1165–1168.
[36] Y.W. Zhang, M.E. Grass, S.E. Habas, F. Tao, T.F. Zhang, P.D. Yang, G.A. Somorjai, J. Phys. Chem. C 111 (2007) 12243–12253.
[37] B. Chaudret, Actualite Chim. (1996) 26–35.
[38] M.L. Kahn, A. Glaria, C. Pages, M. Monge, L. Saint Macary, A. Maisonnat, B. Chaudret, J. Mater. Chem. 19 (2009) 4044–4060.
[39] D.A.J.M. Ligthart, R.A. van Santen, E.J.M. Hensen, Angew. Chem. Int. Ed. 50 (2011) 5306–5310.
[40] D.A.J.M. Ligthart, R.A. van Santen, E.J.M. Hensen, J. Catal. 280 (2011) 206–220.
[41] X. Yang, N. Yan, Z. Fei, R.M. Crespo-Quesada, G.b. Laurenczy, L. Kiwi-Minsker, Y. Kou, Y. Li, P.J. Dyson, Inorg. Chem. 47 (2008) 7444–7446.
[42] S.D. Jackson, L.A. Shaw, Appl. Catal. A 134 (1996) 91–99.
[43] A.M. Goda, M. Neurock, M.A. Barteau, J.G. Chen, Surf. Sci. 602 (2008) 2513–2523.
[44] I. Horiuti, M. Polanyi, Trans. Faraday Soc. 30 (1934) 1164–1172.
[45] G. Iucci, V. Carravetta, G. Paolucci, A. Goldoni, M.V. Russo, G. Polzonetti, Chem. Phys. 310 (2005) 43–49.
[46] V. Carravetta, G. Iucci, A. Ferri, M.V. Russo, S. Stranges, M. de Simone, G. Polzonetti, Chem. Phys. 264 (2001) 175–186.